Sintering temperature dependency on sodium-ion conductivity for $Na_2Zn_2TeO_6$ solid electrolyte

Akihiro Itaya, Kazuki Yamamoto, Ryoji Inada*

Department of Electrical and Electronic Information Engineering, Toyohashi University of Technology,

1-1 Hibarigaoka, Tempaku-cho, Toyohashi, Aichi 441-8580, Japan.

*Corresponding author:

Phone: +81-532-44-6723, Fax: +81-532-44-6757, E-mail address: inada.ryoji.qr@tut.jp

ORCID ID: 0000-0002-6357-092X

ABSTRACT

We investigated the sintering temperature dependency on the properties of $Na_2Zn_2TeO_6$ (NZTO) solid electrolyte synthesized via a conventional solid state reaction method. Sintering temperature of calcined NZTO powder, which was obtained by the calcination of precursor at 850 ºC, was changed in the range from 650 ºC to 850 ºC. XRD analysis showed that P2-type layered NZTO phase was formed in all sintered samples without forming any secondary phases. The relative densities of sintered NZTO samples were approximately 83–85 % for the samples sintered at 700 ºC or higher. The all sintered samples showed sodium-ion conductivity above 10^{-4} S cm^{-1} at room temperature and the highest conductivity of 4.0×10^{-4} S cm^{-1} in the sample sintered at 750 °C. The sintering temperature to obtain the highest room temperature conductivity is 100 ºC lower than that

used in previous works. Such low sintering temperature compared to other Na-based oxide solid electrolytes could be useful for co-sintering with electrode active materials for fabrication of all-solid-state sodium-ion battery.

KEYWORDS: solid electrolyte, layered oxide, sodium-ion conductivity, sintering temperature

1. INTRODUCTION

All-solid-state sodium (Na) ion batteries (SiBs) are promising high-safety and low cost alternatives to current lithium (Li) ion batteries (LiBs), particularly suitable for the application to large-scale energy storage systems.[1–5] Development of inorganic solid Na-ion conducting materials used for solid electrolyte is most critical issue to realize all-solid-state SiBs. The solid electrolyte materials should have not only high Na-ion conductivity above 10^{-3} S cm^{-1} at room temperature but also chemical and electrochemical stabilities against both positive and negative electrode active materials. Although oxide based solid electrolyte materials have rather lower conductivity and poorer deformability than sulfide based one, they have other advantages such as their chemical stability in air and easiness for handling.[3–5]

Na-ion conducting oxide solid electrolyte $Na_2Zn_2TeO_6$ (NZTO) with a P2-type layered structure is an attractive candidate for the application to all-solid-state SiBs, because of the high ionic conductivity above 10^{-4} S cm^{-1} at room temperature range and excellent chemical and electrochemical stability against Na metal.[6–11] NZTO has a honeycomb-structured compound with a space group of $P6_322$ and in the layers, every TeO_6 octahedron is surrounded by six ZnO_6 octahedra via edge-sharing. Na ions are

located between the layers at three different sites, all of which are partially occupied and thus Na ions can migrate among them. In addition, the processing temperature of NZTO is much lower than other Na-ion conducting oxides such as Na-β/β" alumina and NaSICON-type $Na_3Zr_2Si_2PO_{12}$.[12–18]

In the previous works, sintering temperatures of NZTO were commonly set to 850–900 ºC.[6–11] However, this sintering temperature may be still high not only for the Na volatilization in the precursor,[10,11] but also for co-sintering with electrode active materials with similar layered structure for fabricating oxide-based solid-state Na batteries.[19–24] In this paper, we investigated the sintering temperature dependency on the properties of NZTO. We controlled the sintering temperatures at 650–850 ºC and found that all sintered samples show Na-ion conductivity above 10^{-4} S cm^{-1} at room temperature. The maximum room temperature conductivity was achieved when sintering temperature was set to 750 ºC.

2. EXPERIMENTAL

NZTO was synthesized via a conventional solid state reaction method. Na_2CO_3 (Kojundo Chemical Laboratory, 99.5%), ZnO (Kishida Chemical, 99.99%) and TeO_2 (Kojundo Chemical Laboratory, 99.9%) weighed with the molar ratio of Na : Zn : Te = 2.2 : 2 : 1 (adding 10% excess Na taking into account the volatilization of Na during the processing [10,11]) were mixed and ground with ethanol for 5 hours by planetary ball-milling (Nagao System, Planet M2-3F) with zirconia balls with the diameter of 10 mm in a zirconia pot. The mixture was dried at 80 °C and then calcined at 850 °C for 6 hours in air using a SiC crucible. It is noted that the calcination temperature was set to suppress the formation of O'3-type NZTO phase with much lower Na-ion conductivity than P2-

type one.[10] The calcined NZTO powders were reground and pelletized by cold isostatic pressing at 300 MPa, and then sintered at different temperatures of 650, 700, 750, 800 and 850°C for 12 hours in air using a SiC crucible.

The relative densities of all sintered NZTO were calculated by dividing the mass density by the theoretical one (= 4.88 g cm^{-3}).[6,7] The crystal phase of each sintered NZTO was evaluated by X-ray diffraction (XRD, RIGAKU Multiflex) using Cu$K\alpha$ radiation (λ = 0.15418 nm). Microstructure of each sintered NZTO was observed by a scanning electron microscope (SEM, Keyence VE-8800). Ionic conductivity was evaluated at a temperature range from 27 to 127 °C by an AC impedance measurement with a frequency from 4 Hz to 2 MHz and an applied voltage amplitude of 0.1 V, using an impedance meter (HIOKI IM3536). Before the conductivity measurements, both parallel end surfaces of each sintered NZTO pellet were coated with Au films as ion blocking electrodes.

3. RESULTS AND DISCUSSION

XRD patterns for calcined NZTO powder (before sintering) and all NZTO samples with different sintering temperatures are shown in Figure. 1. The calculated patterns for P2-type and O'3-type NZTO phases based on their structure data are also plotted as the references.[6,10] Although the diffraction peaks of the crystal plane with a *c*-axis orientation are emphasized slightly, the peak position from main phase for all sintered samples agrees well with the calculated pattern for P2-type NZTO phase. It is confirmed that the contamination of O'3 phase was negligible, because only the sintering temperatures were changed in the range from 650 to 850 ºC but the calcination temperature of the mixture of starting materials was fixed to 850 ºC.[10]

Figure 2 shows the relative density of NZTO samples plotted against the sintering

temperatures. The relative densities of NZTO samples sintered at 700 ºC or higher were ranged in 83–85 % but the density of the sample sintered at 650 ºC is much lower than others, indicating that the densification of NZTO promotes at temperature above 700 ºC in a conventional solid-state reaction process. SEM images of fractured cross sectional surfaces for all NZTO samples are summarized in Figure 3. NZTO sample sintered at the lowest temperature of 650 ºC are mainly composed of small grains with the size of 1–5 μm (Figure 3(a)). Although the relative densities for the samples sintered at 700 ºC or higher were nearly the same level, several large grains with the size of 10 μm are confirmed in the sample sintered at 850 ºC (Figure 3(e)).

Figure 4(a)–(e) shows the Nyquist plots for electrochemical impedance for all sintered NZTO samples at room temperature (27°C). Here, *Z*' in a horizontal axis and *Z*" in a vertical axis are the real and imaginary parts of impedance, and the units for both components are Ω cm for direct comparison among the samples with different geometrical parameters. It is evident that the plots for all samples are composed of the part of a distorted semicircle at frequency range above several 10 kHz and a linear tail at low frequency range. These data belong to the ionic conduction at NZTO grain boundaries and the response by ionic blocking electrodes, respectively.[11] The characteristic frequencies at which the *Z*" value shows the maximum in a distorted semicircle part are confirmed to be in the range from 0.5 to 0.9 MHz. Since the upper limit of measurement frequency in this work was limited to 2 MHz, the data reflecting the ionic conduction in NZTO grain is not observed clearly. The dashed lines in the graphs (a)–(e) represent the fitting curves for the complex impedance data for the ionic conduction at grain-boundary and the diameter of the fitting line corresponds to the grain-boundary resistivity R_{gb} in each sample. R_{gb} for the sample sintered at 650 ºC is estimated

to be 3600 Ω cm and much larger than other samples, due to the lowest relative density and poor connectivity among the grains. As the sintering temperature increases to 750 or 800 ºC, R_{gb} decreases to 1100–1200 Ω cm. The reduction of R_{gb} with increasing the sintering temperature below 800 ºC is caused by the densification and improvements in intergranular connectivity. At the sintering temperature of 850 ºC, however, R_{gb} is estimated to be approximately 2000 Ω cm and becomes larger than the samples sintered at 750 or 800 ºC. Increase in R_{gb} observed in the sample sintered at 850 ºC may be caused by the formation of very small amounts of secondary phases formed on the NZTO grain surface due to excess Na volatilization from grains reported in our previous work.[11] The capacitance C_{gb} at grain boundary for each sintered NZTO sample is calculated using the relation $C_{gb} = (2\pi f_{max} R_{gb})^{-1}$ (unit of R_{gb} is Ω and f_{max} is characteristic frequency) and estimated to be 10^{-10}–10^{-9} F, which is typical capacitance value for grain-boundary in polycrystalline ceramic materials.

The intercept point of an extrapolation line of the linear tail in low frequency range and horizontal *Z*' axis corresponds to the total (grain + grain boundary) resistivity R_{total} of each sample. The effect of sintering temperature on the R_{gb} contribution in R_{total} are shown in Figure. 4(f). The R_{gb} / R_{total} value in sintered NZTO shows the maximum (= 0.74) at sintering temperature of 650 ºC and minimum (= 0.54) at sintering temperature of 750 or 800ºC. Since the contribution of R_{gb} in R_{total} for sintered NZTO is large, the magnitude relationship of R_{total} among the samples are determined by the difference in R_{gb}. As results, R_{total} shows the maximum (= 4900 Ω cm) in the sample sintered at 650 ºC and the minimum (= 2500 Ω cm) in the sample sintered at 750 ºC. The grain resistivity R_b in each sample is roughly estimated to 1100–1300 Ω cm from by subtracting R_{gb} from R_{total}. The difference in R_b among the samples is not so large compared to R_{gb}, suggesting that the

ionic conductivity of NZTO grain is not influenced so much by the sintering temperature.

Total (grain + grain boundary) ionic conductivity σ_{total} of each NZTO sample is calculated by the R_{total} value estimated in Figure. 4. Figure. 5(a) shows variation of the product of σ_{total} and measurement temperature T for all sintered NZTO as a function of inverse of temperature T. It is confirmed that the temperature dependence of σ_{total} in each sample is well expressed by the Arrhenius equation $\sigma_{total}T = \sigma_0 \exp(-E_a / k_BT)$. Here, σ_0 is constant, E_a is activation energy of conductivity and k_B is Boltzmann constant (= 1.381×10^{-23} J K^{-1}), respectively. E_a of each sample can be estimated from the slope of $\sigma_{total}T$ in Figure. 5(a). E_a tends to decrease with increasing the sintering temperature and shows the minimum (= 0.25 eV) in the sample sintered at 850 °C, but the difference among the samples are not so large. σ_{total} at 27 ºC and E_a for sintered NZTO are also shown in Figure. 5(b), plotted against the sintering temperatures. As shown in Figure. 4, the difference in σ_{total} of sintered NZTO samples are mainly caused by the difference in ionic conduction at the grain boundary depending on the sintering temperature. σ_{total} shows the maximum (= 4×10^{-4} S cm^{-1}) in the samples sintered at 750 °C, which is 100 °C lower than the condition in previous works. [6–11] Such low sintering temperature compared to other Na-based oxide solid electrolytes could be useful for co-sintering with electrode active materials with similar layered structure for fabricating oxide-based all-solid-state SiBs.[19–24] Even for the sample sintered at the lowest temperature of 650 °C, $\sigma_{total} = 2 \times 10^{-4}$ S cm^{-1} was obtained. The lowest σ_{total} of this sample is attributed to the largest grain boundary resistance (Figure. 4(a)), due to the lowest density and poor connectivity among the grains. σ_{total} for the sample sintered at 850 °C was 3.2×10^{-4} S cm^{-1} and slightly lower than the maximum value because of the increase in grain boundary resistance (Figure.

4(e)).

4. CONCLUSION

In conclusion, the sintering temperature dependency on the property for NZTO solid electrolyte was investigated. Sintering temperature of NZTO powder was changed in the range between 650 ºC and 850 ºC. XRD analysis showed that P2-type layered NZTO phase were formed for all sintered samples. When the sintering temperatures is above 700 ºC, the relative densities of NZTO samples attained to 83–85 %. The all sintered samples showed Na-ion conductivity well above 10^{-4} S cm^{-1} at room temperature and the highest conductivity of 4.0×10^{-4} S cm^{-1} was obtained in the samples sintered at 750 ºC. The sintering temperature to obtain the highest room temperature conductivity is 100 ºC lower than that used in previous works for NZTO, and such low sintering temperature could be useful for co-sintering with electrode active materials in oxide-based all-solid-state SiBs.

ACKNOWLEDGEMENTS

This work was partly supported by Research Grant from Iketani Science and Technology Foundation (0321104-A), Foundation of Public Interest of Tatematsu and The Kazuchika Okura Memorial Foundation. We acknowledged the support of the Cooperative Research Facility Center at Toyohashi University of Technology.

REFERENCES

1. Zhou W, Li Y, Xin S, Goodenough JB. Rechargeable sodium all-solid-state battery. ACS Cent Sci 2017; 3:52–57.
2. Hou W, Guo X, Shen X, Amine K, Yu H, Lu J. Solid electrolytes and interfaces in

all-solid-state sodium batteries: Progress and perspective. Nano Energy 2018; 52:279–291.

3. Zhou C, Bag S, Thangadurai V. Engineering materials for progressive all-solid-state Na batteries. ACS Energy Lett 2018; 3:2181−2198.
4. Chao C, Liu L, Qi X, Lu Y, Wu F, Zhao J, Yu Y, Hu YS, Chen L. Solid-state sodium batteries. Adv Energy Mater 2018; 8:1703012
5. Ma Q, Tietz F. Solid-state electrolyte materials for sodium batteries: Towards practical applications. ChemElectroChem 2020; 7:2693–2713.
6. Evstigneeva MA, Nalbandyan VB, Petrenko AA, Medvedev BS, Kataev AA. A new family of fast sodium ion conductors: $Na_2M_2TeO_6$ (M = Ni, Co, Zn, Mg). Chem Mater 2011; 23:1174–1181.
7. Li Y, Deng Z, Peng J, Chen E, Yu Y, Li X, Luo J, Huang YY, Zhu J, Fang C, Li Q, Han J. A P2-type layered superionic conductor Ga-doped $Na_2Zn_2TeO_6$ for all-solid-state sodium-ion batteries. Chem Eur J 2018; 24:1057–1061.
8. Wu JF, Wang Q, Guo X. Sodium-ion conduction in $Na_2Zn_2TeO_6$ solid electrolytes. J Power Sources 2018; 402:513−518.
9. Deng Z, Gu J, Li Y, Li S, Peng J, Li X, Luo J, Huang YY, Fang C, Li Q, Han J, Huang Y, Zhao Y, Ca-doped $Na_2Zn_2TeO_6$ layered sodium conductor for all-solid-state sodium-ion batteries. Electrochim Acta 2019; 298:121−126.
10. Li X, Bianchini F, Wind J, Pettersen C, Wragg DS, Vajeeston P, Fjellvåg H, Insights into crystal structure and diffusion of biphasic $Na_2Zn_2TeO_6$. ACS Appl Mater Interfaces 2020; 12:28188−28198.
11. Itaya A, Yamamoto K, Inada R, Sakurai Y. Effect of excess Na contents in precursor on the property of $Na_2Zn_2TeO_6$ ceramic solid electrolyte. Mater Lett 2020;

284:128941.

12. Youngblood GE, Miller GR, Gordon RS. Relative effects of phase conversion and grain size on sodium ion conduction in polycrystalline, lithia-stabilized β-alumina. J Am Ceram Soc 1978; 61:86–87.
13. Lu X, Xia G, Lemmon JP, Yang Z. Advanced materials for sodium-beta alumina batteries: Status, challenges and perspectives. J Power Sources 2010; 195:2431–2442.
14. Bay MC, Wang M, Glissa R, Heinz MVF, Sakamoto J, Battaglia C. Sodium Plating from Na β-alumina ceramics at room temperature, paving the way for fast-charging all-solid-state batteries. Adv Energy Mater 2020; 10:1902899.
15. Goodenough JB, Hong HYP, Kafalas JA. Fast Na^+-ion transport in skeleton structure. Mater Res Bull 1976; 11:203–220.
16. Noi K, Suzuki K, Tanibata N, Hayashi A, Tatsumisago M. Liquid-phase sintering of highly Na^+ ion conducting $Na_3Zr_2Si_2PO_{12}$ ceramics using Na_3BO_3 additive. J. Ame Ceram Soc 2018; 101:1255–1265.
17. Narayanan S, Reid S, Butler S, Thangadurai V. Sintering temperature, excess sodium, and phosphorous dependencies on morphology and ionic conductivity of NASICON $Na_3Zr_2Si_2PO_{12}$. Solid State Ionics 2019; 331:22–29.
18. Ma Q, Tsai CL, Wei XK, Heggen M, Tietz F, Irvine JTS, Room temperature demonstration of a sodium superionic conductor with grain conductivity in excess of 0.01 S cm^{-1} and its primary applications in symmetric battery cells. J Mater Chem A 2019; 7:7766–7776.
19. Lin Y, Luo N, Chamas M, Hu C, Grasso S. Sustainable high-entropy ceramics for reversible energy storage: A short review. Int J Appl Ceram Technol. 2021; 00:1–10.

https://doi.org/10.1111/ijac.13762.

20. Gupta A, Mullins CB, Goodenough JB. $Na_2Ni_2TeO_6$: Evaluation as a cathode for sodium battery. J Power Sources 2013; 243:817–821.
21. Yang Z, Jiang Y, Deng L, Wang T, Cheng S, Huang Y. A high-voltage honeycomb-layered Na_4NiTeO_6 as cathode material for Na-ion batteries. J Power Sources 2017; 360:319–323.
22. Xiao L, Ding Z, Cheng C, Han Z, Wang P, Huang Q, Gao P, Wei W. Insight into the structural disorder in honeycomb-ordered sodium-layered oxide cathodes. iScience 2020; 23:100898.
23. Kanyolo GM, Masese T, Matsubara M, Chen CY, Rizell J, Huang ZD, Sassa Y, Månsson M, Senoh H, Matsumoto H. Honeycomb layered oxides: structure, energy storage, transport, topology and relevant insights. Chem Soc Rev 2021; 50:3990–4030.
24. Masese T, Miyazaki Y, Rizell J, Kanyolo GM, Takahashi T, Ito N, Senoh H, Saito T. Unveiling structural disorders in honeycomb layered oxide: $Na_2Ni_2TeO_6$, Materialia 2021; 15:101003.

FIGURE CAPTIONS

FIGURE 1. XRD patterns of (a) calcined NZTO powder (before sintering) and (b) NZTO sintered at different temperatures. Calculated patterns for P2-type and O'3-type NZTO phases are also plotted in each graph.[6,10]

FIGURE 2. Relative densities of NZTO plotted against the sintering temperatures. Theoretical density of 4.88 g cm^{-3} are used for the calculation.[6,7]

FIGURE 3. SEM images for fractured surface microstructures of NZTO sintered at different temperatures: (a) 650 ºC, (b) 700 ºC, (c) 750 ºC, (d) 800 ºC and (e) 850ºC.

FIGURE 4. Nyquist plots of AC impedance at 27ºC for NZTO sintered at different temperatures: (a) 650 °C, (b) 700 °C, (c) 750 °C, (d) 800 °C and (e) 850 ºC. The dashed lines in the graphs (a)–(e) are the fitting curves for the complex impedance data at grain-boundary ionic conduction. The contribution of R_{gb} in R_{total} is also plotted against the sintering temperature in (f).

FIGURE 5. (a) Arrhenius plots for all sintered NZTO with different sintering temperatures. The conductivity at 27ºC and activation energy for NZTO are also shown in (b), plotted against the sintering temperatures.

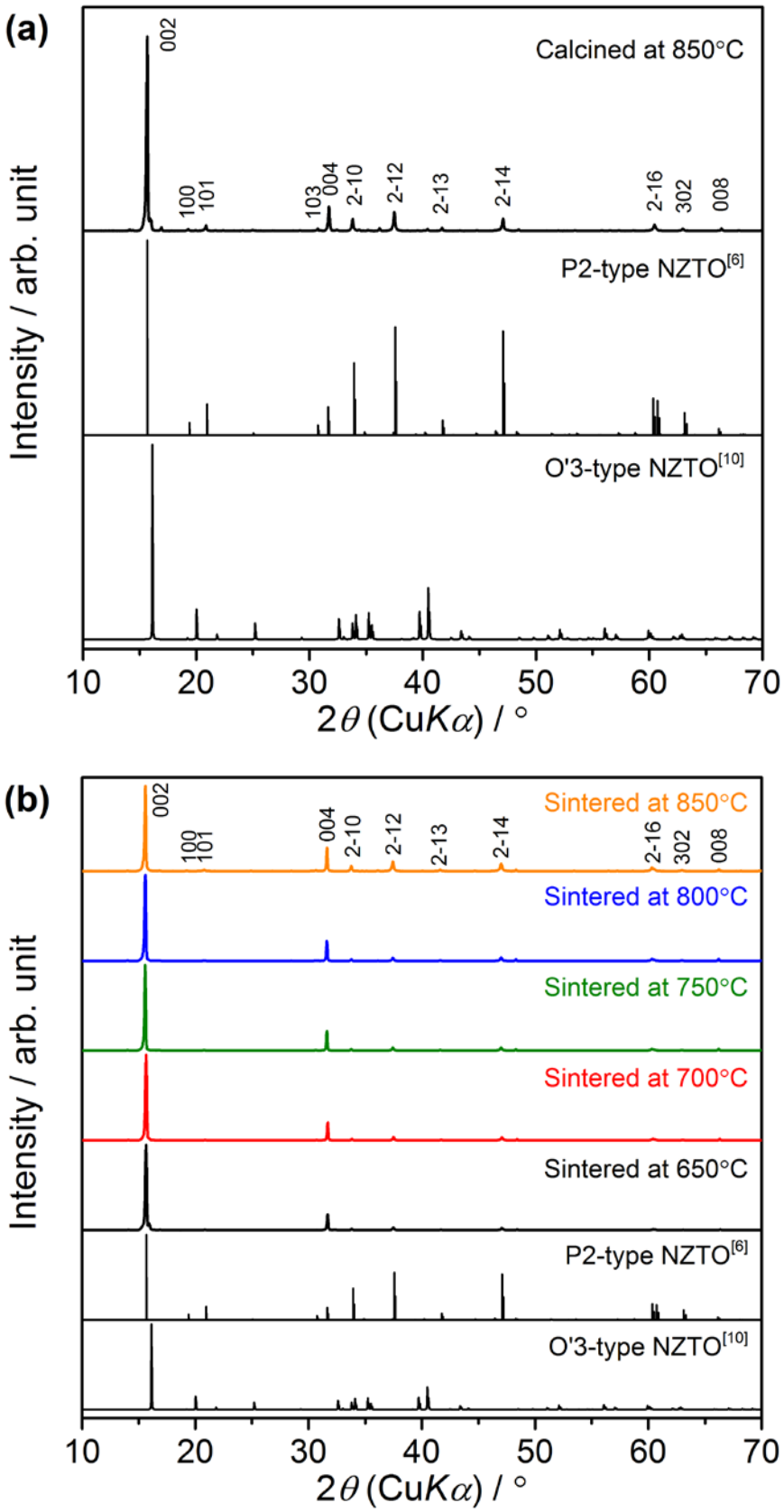
(a)
Calcined at 850°C
P2-type NZTO[6]
O'3-type NZTO[10]
002
100
101
103
004
2-10
2-12
2-13
2-14
2-16
302
008
Intensity / arb. unit
10
20
30
40
50
60
70
2θ (CuKα) / °
(b)
Sintered at 850°C
Sintered at 800°C
Sintered at 750°C
Sintered at 700°C
Sintered at 650°C
P2-type NZTO[6]
O'3-type NZTO[10]
002
100
101
004
2-10
2-12
2-13
2-14
2-16
302
008
Intensity / arb. unit
10
20
30
40
50
60
70
2θ (CuKα) / °

FIGURE 1

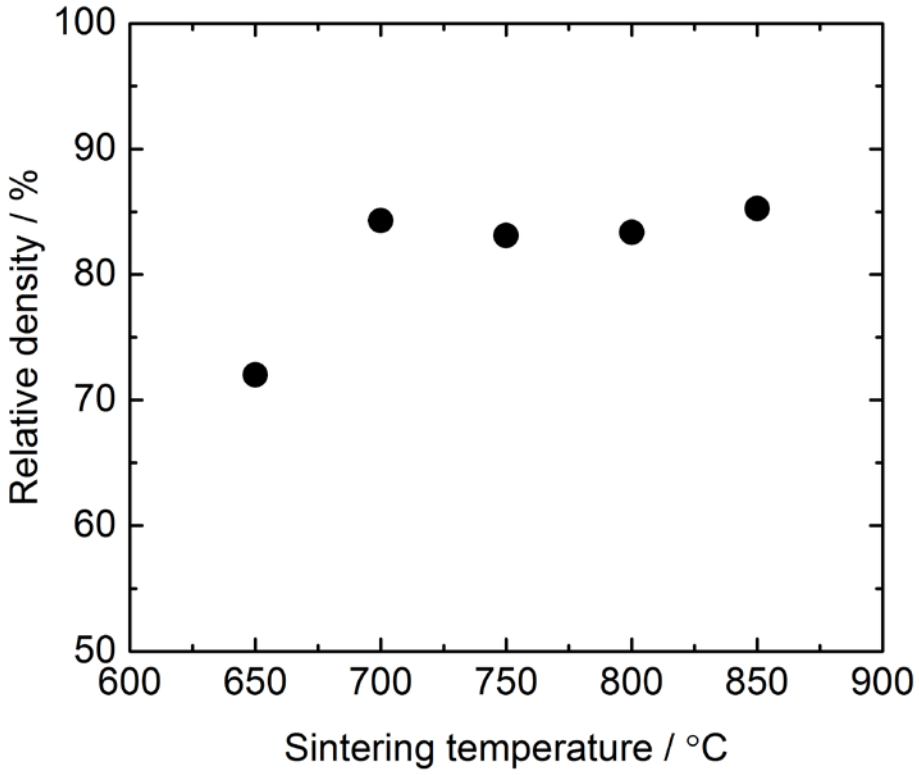
Relative density / %
100
90
80
70
60
50
600
650
700
750
800
850
900
Sintering temperature / °C

FIGURE 2

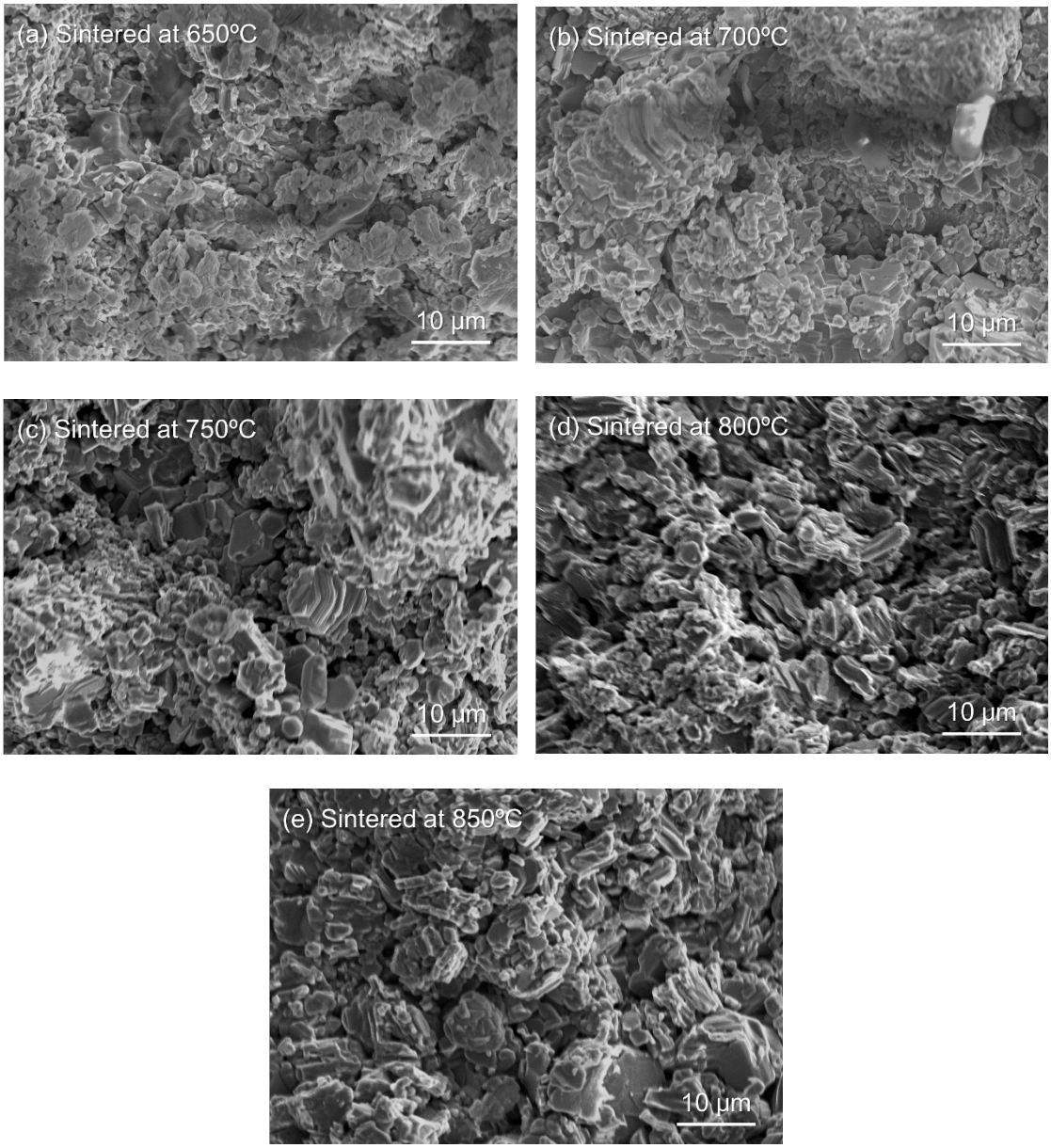
(a) Sintered at 650ºC
10 µm
(b) Sintered at 700ºC
10 µm
(c) Sintered at 750ºC
10 µm
(d) Sintered at 800ºC
10 µm
(e) Sintered at 850ºC
10 µm

FIGURE 3

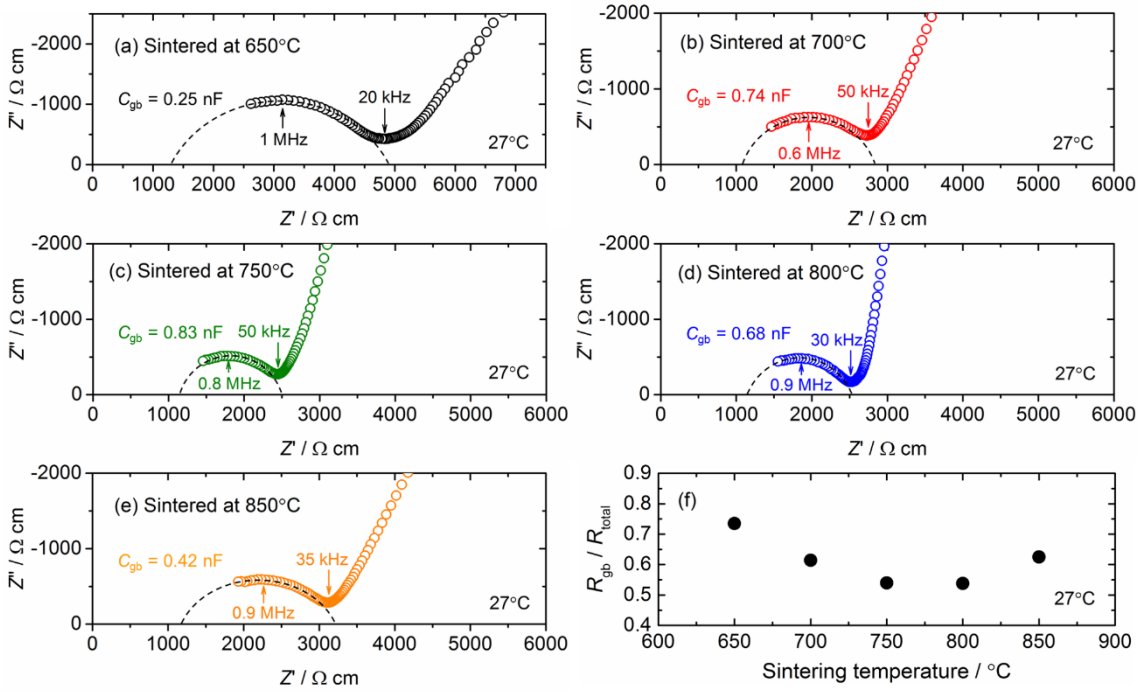
(a) Sintered at 650°C
C_{gb} = 0.25 nF
20 kHz
1 MHz
27°C
(b) Sintered at 700°C
C_{gb} = 0.74 nF
50 kHz
0.6 MHz
27°C
(c) Sintered at 750°C
C_{gb} = 0.83 nF
50 kHz
0.8 MHz
27°C
(d) Sintered at 800°C
C_{gb} = 0.68 nF
30 kHz
0.9 MHz
27°C
(e) Sintered at 850°C
C_{gb} = 0.42 nF
35 kHz
0.9 MHz
27°C
Z'' / Ω cm
Z' / Ω cm
(f)
R_{gb} / R_{total}
Sintering temperature / °C

FIGURE 4

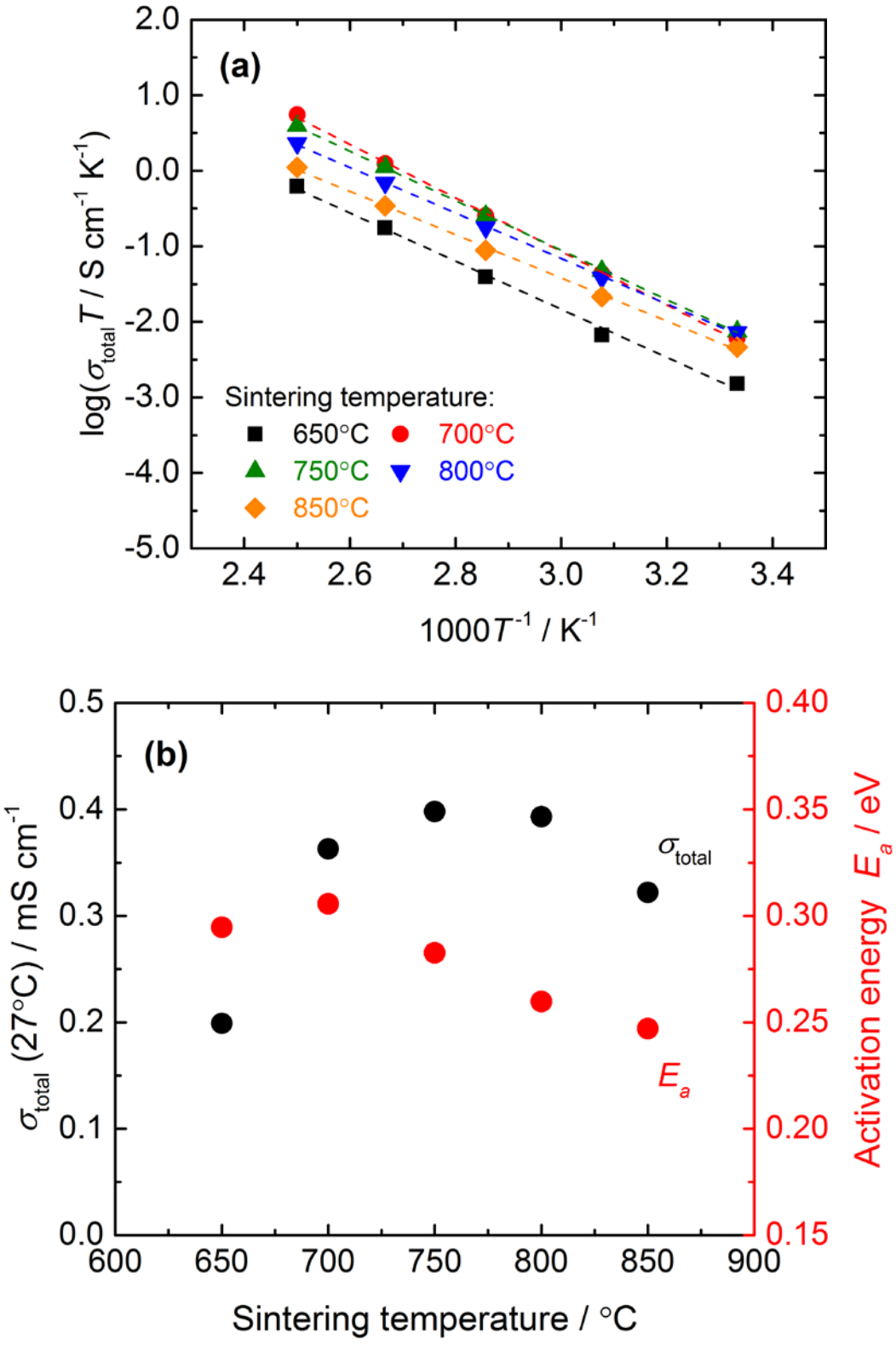
(a)
log(σtotal T / S cm-1 K-1)
1000T-1 / K-1
Sintering temperature:
650°C
700°C
750°C
800°C
850°C
(b)
σtotal (27°C) / mS cm-1
Activation energy Ea / eV
σtotal
Ea
Sintering temperature / °C

FIGURE 5